HHS Public Access

Author manuscript

Nat Struct Mol Biol. Author manuscript; available in PMC 2019 September 04.

Published in final edited form as:

Nat Struct Mol Biol. 2019 March ; 26(3): 213–219. doi:10.1038/s41594-019-0192-3.

The macroH2A1.2 histone variant links ATRX loss to alternative telomere lengthening.

Jeongkyu Kim[1,7], **Chongkui Sun**[2,7], **Andy D. Tran**[1], **Pei-Ju Chin**[2,6], **Penelope D. Ruiz**[3], **Kun Wang**[2], **Richard J. Gibbons**[5], **Mathew J. Gamble**[3,4], **Yie Liu**[2,*], and **Philipp Oberdoerffer**[1,*]

[1]Laboratory of Receptor Biology and Gene Expression, National Cancer Institute, NIH, Bethesda, Maryland, USA.

[2]Laboratory of Molecular Gerontology, National Institute on Aging, NIH, Baltimore, Maryland, USA.

[3]Department of Molecular Pharmacology, Albert Einstein College of Medicine, Bronx, New York, USA.

[4]Department of Cell Biology, Albert Einstein College of Medicine, Bronx, New York, USA.

[5]Medical Research Council, Molecular Hematology Unit, Weatherall Institute of Molecular Medicine, University of Oxford, John Radcliff Hospital, Oxford OX3 9DS, UK.

[6]Present address: Tissue Microbiology Laboratory, Food and Drug Administration, Silver Spring, Maryland, USA.

[7]These authors contributed equally.

Abstract

The growth of telomerase-deficient cancers depends on the alternative lengthening of telomeres (ALT), a homology-directed telomere maintenance pathway. ALT telomeres exhibit a unique chromatin environment and generally lack the nucleosome remodeler ATRX, pointing to an epigenetic basis for ALT. Recently, we have identified a protective role for the ATRX-interacting macroH2A1.2 histone variant during homologous recombination (HR) and replication stress (RS). Consistent with an inherent susceptibility to RS, we show that human ALT telomeres are highly enriched for macroH2A1.2. However, in contrast to ATRX-proficient cells, ALT telomeres transiently lose macroH2A1.2 during acute RS to facilitate DSB formation, a process that is almost completely prevented by ectopic ATRX expression. Telomeric macroH2A1.2 is re-

*Correspondence: Philipp Oberdoerffer, National Cancer Institute, Building 41, Room B907, Bethesda, MD 20892, U.S.A, Philipp.Oberdoerffer@nih.gov, Phone: 301-594-0689, Fax: 301-496-4951; Yie Liu, National Institute on Aging, Laboratory of Molecular Gerontology, Baltimore, MD 21224, U.S.A, liuyie@mail.nih.gov, Phone: 301-594-0689, Fax: 301-496-4951.

Author contributions

J. K., Y.L. and P. O. conceived the project. J. K. performed ChIP, western blot and cell growth analyses, C.S. performed dot plots, Q-FISH, T-SCE and TIF assay, with help from K. W. and P.J. C., A.D.T. performed IF analyses, P. D. R. performed in vitro affinity purification, R. J. G. contributed U2OS-ATRX cells. P. O. wrote the manuscript with help from Y. L. M. J. G., and J. K.

Competing Interests Statement

The authors have no competing interests as defined by Nature Research, or other interests that might be perceived to influence the results and/or discussion reported in this paper.

deposited in a DNA damage response (DDR)-dependent manner to promote HR-associated ALT pathways. Our findings thus identify the dynamic exchange of macroH2A1.2 on chromatin as an epigenetic link between ATRX loss, RS-induced DDR initiation and telomere maintenance via HR.

Introduction

Telomere maintenance is essential for the survival of rapidly dividing tumor cells. To achieve this, tumors either re-express telomerase or undergo alternative lengthening of telomeres (ALT). The latter is a telomerase-independent mechanism that relies on homology-directed telomere maintenance. ALT occurs in 5–15% of human tumors and is generally associated with poor prognosis [1–3]. Perhaps the most consistent indicator of ALT is a functional defect in the chromatin remodeler ATRX [4,5]. Supporting a role for ATRX in ALT, its re-expression was recently shown to suppress ALT hallmarks such as homologous recombination (HR)-dependent telomere sister chromatid exchange (T-SCE) through mechanisms that remain to be fully explored [6–8]. Further supporting a role for chromatin in ALT, loss of the histone chaperone ASF1 resulted in a rapid induction of the ALT phenotype in telomerase-positive cells [9]. Understanding the mechanistic link between chromatin structure and ALT telomere maintenance pathways may, thus, provide essential insight into the molecular pathways that regulate the growth of these malignant tumor types.

Chromatin perturbations in ALT cells are thought to act primarily by increasing replication stress (RS) susceptibility, which in turn promotes DSB formation to trigger HR-dependent telomere lengthening [2]. How these processes are coordinated is a matter of intense investigation. Of note, ATRX is recruited to chromatin upon RS and its depletion aggravates RS-induced replication fork collapse and DSB formation [10]. Moreover, re-expression of ATRX in ALT cells reduces RS-associated DNA damage, implicating ATRX in the resolution of stalled replication forks [6]. With respect to chromatin, ATRX has been linked to the incorporation of two histone variants, H3.3 and macroH2A1 [11–13]. We recently identified macroH2A1.2, one of two structurally distinct alternative macroH2A1 splice isoforms, as a mediator of HR and the replication stress response. Specifically, macroH2A1.2 promotes the recruitment of the tumor suppressor BRCA1 [14–16], which has been implicated in repair pathway choice at DSBs and stalled replication forks, where it facilitates HR as well as break-induced replication (BIR) [17–19]. BIR involves long-tract, conservative DNA synthesis upon DNA break formation and subsequent strand invasion, a process recently found to orchestrate homology-directed telomere maintenance in ALT tumors [20]. Together, these findings raise the intriguing possibility that ATRX loss may affect ALT by modulating the macroH2A1.2 chromatin landscape at telomeres.

Here, we show that macroH2A1.2 is enriched at telomeres, particularly in ALT cells. Consistent with its role as an HR mediator, macroH2A1.2 loss results in defective HR-associated telomere maintenance. Perhaps more importantly, we identify an ATRX-dependent pathway that maintains macroH2A1.2 levels during acute RS, the absence of which accounts for RS-associated DSB formation in ATRX-deficient cells. MacroH2A1.2 thus presents a tightly regulated modulator of both telomere-associated DNA damage

formation and its subsequent homology-directed repair, with direct implications for malignant growth.

Results

MacroH2A1.2 is enriched at telomeres and subtelomeric regions

Given the repetitive nature of telomeric DNA and its propensity to form secondary structures, telomeres are particularly difficult to replicate and, thus, intrinsically prone to RS [1,2]. We recently identified RS as a driver of macroH2A1.2 accumulation at fragile genomic regions [16] and asked if macroH2A1.2 is similarly enriched at and functionally implicated in the maintenance of telomeric DNA. To assess macroH2A1.2 accumulation at chromosome ends, we performed macroH2A1.2 chromatin immunoprecipitation (ChIP) followed by qPCR using primer sequences against unique subtelomeric genomic loci [21]. Compared to non-fragile control loci, macroH2A1.2 was enriched at subtelomeric chromatin in a total of six cell lines tested. MacroH2A1.2 enrichment was most pronounced in telomerase-negative ALT cell lines, which are particularly susceptible to telomeric RS (Fig. 1A) [2]. Using ChIP followed by dot blot to detect TTAGGG telomere repeat DNA, we confirmed abundant macroH2A1.2 occupancy at telomeres in ALT-positive U2OS cells. The telomere-associated shelterin component TRF2 served as a positive control (Fig. 1B). No enrichment was observed upon ChIP with the centromeric CENP-A protein (Fig S1A). Consistent with our previous work [16], we also observed enrichment of macroH2A1.2 relative to input DNA at non-telomeric Alu repeats, which was, however, ~10-fold less pronounced than at telomeres (Fig. S1B). Together, these findings demonstrate that telomeres and subtelomeric regions are marked by the macroH2A1.2 histone variant.

MacroH2A1.2 facilitates HR-dependent telomere maintenance at DSBs

We next sought to investigate if macroH2A1.2 accumulation at telomeres plays a role in telomere maintenance. Consistent with this notion, RNA interference (RNAi)-mediated depletion of macroH2A1.2 resulted in a reduction in telomere signal intensity in two distinct ALT cell lines as measured by quantitative fluorescent in-situ hybridization (Q-FISH) with a telomere-specific DNA probe (Fig. 1C, Fig. S1C-F). SiRNAs were directed against two distinct target sequences within the macroH2A1.2-specific exon 6a (si-1.2–1 or si-1.2–2). The efficiency and splice-variant specificity of RNAi-mediated macroH2A1.2 depletion was confirmed by Western Blot (Fig. S1C). MacroH2A1.2 depletion in the same two ALT cell lines further resulted in a robust decrease in the formation of extrachromosomal telomere $(CCCTAA)_n$ DNA circles (C-circles), which are highly specific to ALT cells, provide a responsive marker of ALT activity [22] and have further been linked to elevated telomeric replication stress [23] (Fig. 1D, Fig. S1G). To allow for efficient C-circle formation, cells were analyzed 6–12 days after stable, shRNA-mediated knockdown, shRNA target sequences were identical to those of siRNAs (Table S1). These data demonstrate that macroH2A1.2 contributes to telomere maintenance and the ALT phenotype.

Consistent with macroH2A1.2 being a mediator of HR at DSBs [14], its depletion resulted in a ~ 2-fold reduction in T-SCE in two distinct ALT cell lines (Fig. 2A, B, Fig. S2A). T-SCE measures homology-directed telomeric gene conversion events via strand-specific labeling

of telomere chromatids to allow for the detection of telomere-specific cross-overs by chromosome orientation fluorescence in situ hybridization (CO-FISH) [24]. To further corroborate a defect in telomeric HR, we assessed the impact of macroH2A1.2 loss on BIR at telomeres. BIR results in de novo DNA synthesis at sites of DSBs following homology-directed invasion of a broken DNA strand in a manner that is distinct from S phase replication [20,25]. BIR was recently identified as a means for DSBs to enact nascent long-tract telomeric DNA synthesis using intact telomeres as a template [20]. BIR can be measured via the immunofluorescence (IF)-based detection of bromodeoxyuridine (BrdU) incorporation. Using an mCherry-TRF1-Fok1 fusion protein, which tethers the Fok1 endonuclease to telomeric repeats via the telomeric protein TRF1 and thus allows for telomere-specific DSB induction [20,26], we measured BrdU intensity at mCherry-TRF1-FokI foci by immunofluorescence (IF). Depletion of macroH2A1.2 with two distinct shRNAs resulted in a robust decrease in BrdU signal (Fig. 2D, E), indicating that macroH2A1.2 promotes BIR at broken telomeres. TRF1-FokI-induced DSB formation was confirmed by the accumulation of S139-phosphorylated histone H2AX (γ-H2AX) at TRF1-FokI foci and was not significantly affected by maroH2A1.2 depletion (Fig. 2F, Fig. S2D). Of note, ALT telomere maintenance has been linked to RS-induced recruitment of BRCA1 [27], which has in turn been implicated in promoting BIR at stalled replication forks [19]. In line with the fact that macroH2A1.2 promotes BRCA1 recruitment at non-telomeric DSBs [14], shRNA-mediated macroH2A1.2 depletion caused a marked decrease in BRCA1 at TRF1-FokI-induced DNA breaks (Fig. 2G, H). Similar results were observed with an independent siRNA (Fig. 2I, S2B, C). Conversely, overexpression of macroH2A1.2 resulted in increased BRCA1 accumulation in the same assay (Fig. 2J, Fig. S2G). Little γ-H2AX or BRCA1 accumulation was observed with a catalytically dead FokI enzyme (FokI-D450A), demonstrating DSB requirement for efficient DDR activation (Fig. S2F). Of note, BRCA1 recruitment to telomeric DSBs remained largely unaltered upon depletion of the alternative macroH2A1.1 splice isoform (Fig. S2H). Moreover, depletion of macroH2A1.1 did not impair HR in a reporter assay (Fig S2I). These observations emphasize the existence of unique, splice variant-specific functions of macroH2A1 isoforms, and a detailed dissection of the underlying molecular basis will be an important aspect of future investigations. Together, these findings demonstrate that macroH2A1.2 promotes HR-mediated telomere maintenance, which is correlated with BRCA1 recruitment to telomeric DSBs.

RS promotes acute macroH2A1.2 loss at telomeres of ATRX-deficient cells

Given the protective role for macroH2A1.2 during RS [16], abundant, HR-permissive macroH2A1.2 levels at ALT telomeres are seemingly at odds with their increased susceptibility to RS. We, thus, asked whether RS may alter macroH2A1.2 occupancy at ALT telomeres to promote a more RS-prone chromatin environment. Consistent with this notion, exposure of U2OS cells to low levels of the ribonucleotide reductase inhibitor and replication poison hydroxyurea (HU) caused a > 10-fold loss of subtelomere-associated macroH2A1.2 relative to its nucleosomal binding partner H2B by ChIP analysis (Fig. 3A). H2B levels were not significantly affected by RS or ATRX expression (Fig. S3A). RS-induced macroH2A1.2 loss at telomeres was confirmed by telomere-specific dot blot (Fig. 3B). Similar results were observed in two additional ALT cell lines (Fig. S3C, D) and with a distinct source of RS, the DNA polymerase inhibitor aphidicolin (Aph) (Fig. S3B). No major

macroH2A1.2 loss was detected at a non-fragile control locus, pointing to an RS-specific change in chromatin (Fig. 3A, Fig. S3B, C). Moreover, telomerase-positive tumor cell lines showed little to no RS-induced telomeric macroH2A1.2 loss, suggesting that this phenomenon is specific to ALT cells (Fig. S3C). Given that most ALT cell lines including those tested here lack expression of the nucleosome remodeler and macroH2A1.2 interactor ATRX [12,28], we asked if the absence of ATRX is functionally linked to RS-induced macroH2A1.2 loss at telomeres. To do so, we took advantage of a doxycycline-inducible system for ATRX re-expression in U2OS cells, which was shown to repress several hallmarks of ALT through yet to be defined mechanisms [6]. Notably, restoration of ATRX almost completely rescued the HU-induced macroH2A1.2 loss, as determined by both ChIP at distinct subtelomeric loci and telomere-specific dot blot (Fig. 3A, B). Conversely, ATRX depletion in ALT-negative K562 cells resulted in RS-induced loss of subtelomeric and telomeric macroH2A1.2, whereas canonical H2A and H2B histones remained largely unaltered (Fig. 3C, Fig. S3E, F). Affinity purification of recombinant histone dimers containing H2B and either H2A or the histone-like region of macroH2A1 (mH2A1$^{1-122}$) revealed that ATRX preferentially interacts with the histone-domain of macroH2A1, supporting a role for ATRX in macroH2A1 variant-specific nucleosome remodeling (Fig. 3D). ATRX deficiency does, however, not generally interfere with macroH2A1.2 accumulation at telomeres, as macroH2A1.2 is abundant at these genomic loci in the absence of RS both in ALT-positive cell lines and ATRX-depleted K562 cells (Fig. 3A-C, Fig. S3C-F). Together, these observations point to a unique, RS-specific role for ATRX in macroH2A1.2 maintenance at telomeres that is distinct from its impact on chromatin in the absence of damage.

DNA damage signaling and ATRX coordinate RS-associated macroH2A1.2 remodeling

Given the abundance of macroH2A1.2 at ALT telomeres, we reasoned that mechanisms must exist to counteract RS-induced macroH2A1.2 loss. In ATRX-proficient cells, macroH2A1.2 accumulation at sites of RS is controlled by DDR signaling [16]. We, thus, sought to determine if the DDR similarly affects macroH2A1.2 levels at ALT telomeres. Consistent with this notion, inhibition of ATM- or ATR-signaling significantly exacerbated macroH2A1.2 loss during HU treatment in ALT cells, indicating that DDR signaling counteracts RS-induced macroH2A1.2 depletion in ATRX-deficient cells. Comparatively minor effects were observed at a non-fragile, non-telomeric control locus, consistent with fragile site-specific macroH2A1.2 reorganization described previously (Fig. 3E, Fig. S3G) [16]. Moreover, in agreement with dynamic macroH2A1.2 depletion and re-accumulation at sites of DSBs [14], we observed a robust recovery of telomeric macroH2A1.2 levels 6 h after HU removal (Fig. 3F). In light of these findings, we propose that macroH2A1.2 deposition at sites of RS involves both ATRX-dependent chromatin remodeling and DDR activation, resulting in transient, RS-specific macroH2A1.2 loss in ATRX-deficient cells.

ATRX prevents macroH2A1.2 loss and concomitant excessive DNA damage

We next sought to determine the impact of RS-associated macroH2A1.2 loss on telomeric DNA break formation. We have previously shown that macroH2A1.2 depletion results in a significant increase in fragile site-associated DNA damage in ATRX-proficient K562 cells [16]. The latter is also the case for subtelomeric loci, which show a marked increase in γ-

H2AX by ChIP in macroH2A1.2 deficient cells (Fig. 4A, Fig. S4A). MacroH2A1.2 ChIP confirmed CRISPR-Cas9-mediated macroH2A1.2 gene inactivation (Fig. S4A) [16]. We next asked if RS-induced macroH2A1.2 loss in ALT cells is similarly related to DSB formation. To do so, we assessed γ-H2AX induction in U2OS cells upon RS in the absence or presence of ATRX re-expression, to allow for or prevent RS-associated macroH2A1.2 loss, respectively. ATRX induction was able to suppress DNA damage at ALT telomeres in response RS, as determined by γ-H2AX ChIP qPCR at subtelomeric loci and by IF for telomere dysfunction induced foci (TIF) (Fig. 4B, C). TIFs are defined as DNA damage-bearing telomeres, which are detected by combining γ-H2AX IF with telomere FISH. To determine if the protective effect of ATRX is dependent on macroH2A1.2, we re-expressed ATRX in the presence or absence of macroH2A1.2 knockdown followed by a quantification of TIF formation. In contrast to macroH2A1.2 proficient cells, ATRX re-expression did not significantly reduce TIFs in macroH2A1.2-depleted cells exposed to RS, supporting the notion that ATRX counteracts RS-induced DNA damage by preventing macroH2A1.2 loss at telomeres (Fig. 4C). ATRX deficiency thus allows for increased RS at ALT telomeres via acute chromatin reorganization involving the transient depletion of macroH2A1.2. Underlining the potential relevance of these findings for ALT tumor growth, stable depletion of macroH2A1.2 caused a progressive, proliferative defect in two independent ALT cell lines (Fig S4B-D), whereas no growth defect was observed in two telomerase-positive and ALT-negative tumor cell lines (Fig. S4E, F).

Discussion

Here, we identify macroH2A1.2 as a telomere-enriched chromatin component that links ATRX loss to HR-dependent telomere maintenance. Our findings are consistent with the following model: By promoting acute loss of macroH2A1.2 during RS, the absence of ATRX causes increased DSB formation to initiate ALT. A dynamic, DDR-dependent re-deposition of macroH2A1.2 at DSBs allows for macroH2A1.2 restoration at telomeres to facilitate homology-directed repair and, thus, promote the execution of ALT (Fig. 4D). Together, these findings provide a mechanistic rationale for ATRX loss in tumors that rely on ALT and identify macroH2A1.2 as a potential therapeutic target for the manipulation of ALT tumor growth.

Changes in telomeric chromatin have previously been implicated in ALT-associated telomere maintenance. The nucleosome remodeling and histone deacetylation (NuRD) complex was shown to promote remodeling of telomeric chromatin to create an environment that facilitates T-SCE [29]. More recently, depletion of ASF1 histone chaperones was found to induce ALT in telomerase-positive tumor cells [9]. However, a mechanistic understanding of the role of chromatin in ALT, particularly with regard to ATRX, one of the most commonly mutated chromatin modulators in ALT cells, is missing [4,5]. Our findings now uncover a central role for an ATRX-associated histone variant, macroH2A1.2, during RS and HR at telomeres. ATRX, together with the DAXX chaperone, has further been implicated in histone H3.3 deposition, which, like ATRX and DAXX, carries potential ALT driver mutations [1,11,13]. It will thus be interesting to determine if changes in macroH2A1.2 and H3.3 deposition can functionally cooperate to modulate RS susceptibility and repair outcome at telomeres of ATRX-deficient cells.

Of note, a previous genome-wide study uncovered an inverse correlation between ATRX and macroH2A1.2 deposition on chromatin [12]. Consistent with this, we observed a modest reduction of macroH2A1.2 at subtelomeric DNA upon ATRX re-expression in the absence of RS (see Fig. 3A), suggesting that ATRX-dependent remodeling of macroH2A1.2 may be differentially regulated in the presence or absence of DNA damage signaling. In support of this notion, ATRX depletion in human cancer cell lines was found to promote DSB formation and replication fork stalling specifically in the presence of RS or DNA damaging agents (Fig. 4D) [10,30]. On the other hand, ATRX inactivation in mouse models and primary mouse cells resulted in replication defects, increased DNA damage and telomere dysfunction even in the absence of exogenous DNA damage, suggesting that endogenous RS may be sufficient to trigger replication defects in these models [13,31–33]. Pointing to cell cycle-associated changes in ATRX function, ATRX and DAXX accumulate on chromatin at the end of S phase, specifically at late replicating and RS-sensitive heterochromatic regions [34]. Moreover, ATRX was shown to be modulated by phosphorylation at the onset of mitosis, a timepoint that has been associated with fragile site-associated metaphase chromosome breaks and gaps [35,36]. It will be important for future work to determine if and how RS affects ATRX function with regard to its chromatin remodeling activities. Similarly, it will be of interest to determine a possible link between ATRX and the FACT chaperone, which we found to promote DDR-dependent macroH2A1.2 reorganization at fragile genomic regions [16].

ATRX interacts not only with macroH2A1.2, but also with its alternative splice isoform macroH2A1.1. The two macroH2A1 variants differ in 33 aa within the macro-domain, which allows macroH2A1.1 but not macroH2A1.2 to bind poly-ADP ribose (PAR) [37]. Interaction with ATRX was shown to prevent macroH2A1.1 from binding to PARylated tankyrase, thus enabling tankyrase to localize to telomeres to resolve sister chromatid cohesion [28]. ATRX loss has, thereby, been linked to persistent telomere cohesion and increased T-SCE. Of note, macroH2A1.1 depletion does not impair HR or BRCA1 accumulation at telomeric DSBs (Fig. S2H, I). We, thus, conclude that, while both macroH2A1 splice variants appear to promote ALT as a result of ATRX loss, they do so via distinct molecular pathways, consistent with differential roles for these variants during other cellular processes, including DSB repair and cell growth [38].

Finally, it is worth noting that macroH2A1.2 is not only enriched at ALT telomeres but also at telomeres of ATRX-expressing, ALT-negative tumor cell lines, albeit at lower levels (Fig. 1A). MacroH2A1.2 function at telomeres is, thus, unlikely restricted to ALT cells. Indeed, experimental deletion of macroH2A1.2 causes aberrant, telomeric DNA damage in ALT-negative cells (Fig. 4A). This genome-protective function of macroH2A1.2 may explain how restoration of ATRX, which prevents telomeric macroH2A1.2 loss upon RS in ALT-positive cells, counteracts the accumulation of the DSB repair effector MRE11 at ALT telomeres [6]. Together, these findings indicate that macroH2A1.2 may be targeted to modulate DNA damage formation and genome instability, particularly in ATRX-deficient ALT tumors, which are often characterized by a poor clinical prognosis.

Methods

Cell lines, viral infection and drug treatments.

U2OS (American Type Culture Collection, ATCC, female), SaOS-2 (ATCC, female), GM(00)847 (Coriell, male), HT1080 (ATCC, male), Hela (ATCC, female) and HEK-293T cells (gift from The Broad Institute) were cultured in DMEM (Gibco) with 10% FBS (Gemini) and 1% penicillin-streptomycin (Gibco). For ATRX expression, U2OS cells carried a stably integrated doxycycline-inducible ATRX transgene (U2OS-ATRX) [6]. For telomeric DSB induction, U2OS cells carried a stably integrated doxycycline-inducible TRF1-FokI or TRF1-FokI-D450A transgene (gift from R. Greenberg) [26]. K562 cells (ATCC, female) were cultured in RPMI1640 (Gibco) with 10% BCS (Hyclone). All cells were cultured at 37 °C in a humidified incubator containing 5% CO_2. Cell lines were negative for mycoplasma. ShRNA expressing lentiviral infections were performed by spin infection (2250 rpm, 75 min, Beckman-Coulter Allegra X-12R centrifuge) with 8 μg/ml polybrene (Sigma), followed by incubation overnight prior to virus removal and selection with 2 μg/ml puromycin. Unless noted otherwise, cells were analyzed within 7 days of infection. Individual MISSION shRNA-expressing lentiviral vectors were from Sigma (Table S1). SiRNAs (Dharmacon ON-TARGET, Table S1) were transfected using DF-1 reagent following the manufacturer's instructions (Dharmacon) and analyzed at 48 – 72 h post transfection. For T-SCE and telomere length analyses, cells were transfected with 40 nM of the indicated siRNA using INTERFERin transfection reagent (Polyplus, Cat# 409–10) and analyzed 64 h thereafter. For macroH2A1.2 overexpression, U2OS TRF1-Fok1 cells were infected with pLVX-puro-eGFP or FLAG-macroH2A1.2 lentivirus by spin-infection as described above. Cells were analyzed within 7 days post infection. Drug treatments were carried out as follows: Unless otherwise noted, doxycyclin was administered at 0.4 μg/ml for 72 h, HU (Sigma) and Aph (Sigma) for 24 h at 0.3 mM and 0.5 μM, respectively. ATM inhibitor KU-55933 (Calbiochem) or ATR inhibitor VE-821 (AdooQ Bioscience) were added at a concentration of 10 μM 30 min prior to Aph or HU treatment.

TRF1-Fok1 immunofluorescence.

Expression of mCherry-TRF1-Fok1 was induced in U2OS TRF1-Fok1 cells using 40 ng ml $^{-1}$ doxycycline for 24 hours. Following doxycycline induction, TRF1-Fok1 was stabilized and translocated to the nucleus using 1 μM Shield-1 (Takara Clontech) and 1 μM 4-hydroxytamoxifen (4-OHT) (Sigma-Aldrich) for 2 hours. Cells were then fixed in PBS + 2% PFA, followed by permeabilization in PBS + 0.5% TritonX-100. Cells were subsequently blocked in 5% BSA in PBS + 0.1% Tween-20 (PBS-T). For BrdU immunofluorescence, U2OS TRF-Fok1 cells were pulsed with 100 μM BrdU (BD Biosciences) along with Shield-1 and 4-OHT for 2 hrs. Cells were then fixed in PBS + 4% PFA, followed by permeabilization in PBS + 0.5% TritonX-100. Cells were denatured in 500 U ml^{-1} DNaseI (Roche) in 1x reaction buffer (20mM Tris-HCl (pH 8.4), 2 mM $MgCl_2$, 50 mM KCL in PBS-T) for 25 min at 37°C in a humidified chamber. Primary and secondary antibody stainings were carried out in PBS-T. Confocal *z*-stacks were acquired using a Zeiss LSM 780 microscope and a 40x oil objective (NA=1.4). Images were displayed and analyzed as maximum intensity projections. Analysis of $BrdU^+$ foci was limited to non-S phase cells, as defined by lack of pan-nuclear BrdU staining, all other analyses were performed in

asynchronous cells. Enrichment of γ-H2AX$^+$, BRCA1 or BrdU was determined by measuring the fluorescence intensity at mCherry-labeled TRF1 foci relative to total nuclear intensity. Foci were defined as BrdU$^+$, BRCA1$^+$ or γ-H2AX$^+$, when the signal intensity at TRF1 foci was more than 2-fold greater that total nuclear signal intensity. This threshold was determined based on background enrichment detected upon expression of catalytic dead TRFI-FokI-D450A (Fig. S2F).

Detection of telomere dysfunction-induced foci (TIFs).

Control and macroH2A1.2 knockdown U2OS-ATRX cells were induced for ATRX expression with doxycycline for 24 hours, followed by 1 mM Aphidicolin treatment for 18 hours. Cells were fixed with 4% formaldehyde at 4°C, permeabilized with 0.5 % Triton X-100, and blocked with 3% BSA. Cells were immunostained with primary antibodies, followed by Alexa Fluor-labeled secondary antibody (1:500; Invitrogen) for 1 h at 37 °C. Images were acquired on an Axio2 microscope (Zeiss) and scored manually for TIFs, measured by the colocalization of γ-H2AX and TRF2.

Antibodies.

The following antibodies were used for ChIP: α-macroH2A1.2 (Millipore MABE61), α-phospho-S139-H2AX (Millipore 05–636), α-H2B (Abcam ab52484), α-H2A (Abcam ab18255), TRF2 (Novus Biologicals IMG-124A) and normal mouse IgG (Millipore 12–371). Primary antibodies for western blotting were: α-macroH2A1.2 (Millipore MABE61), α-phospho-S139-H2AX (S139) (Millipore 05–636), α-BRCA1 (Santa Cruz sc-6954), α-ATRX (Cell signaling 14820s), α-GAPDH (Santa Cruz sc-32233), α-H2AX (Abcam ab20669). Secondary antibodies were goat anti-mouse IgG (H+L)-HRP (Invitrogen 31430) and goat anti-rabbit IgG (H+L)-HRP (Invitrogen 31460). Primary antibodies for IF were α-BRCA1 (Santa Cruz sc-6954), α-γ-H2AX (Millipore 05–636, Abcam ab11174), α-BrdU (BD Biosciences 555627), and TRF2 (Novus Biologicals IMG-124A), secondary antibodies were goat-anti-mouse or goat-anti-rabbit IgG (H+L) coupled to Alexa Fluor 488 or 647 (Life Technologies).

Western blotting.

Cells were lysed with RIPA lysis buffer (150 mM NaCl, 1% NP-40, 1% Na-deoxycholate, 0.1% SDS, 25 mM Tris-HCl pH 7.5) with protease inhibitor cocktail (Roche cOmplete) and phosphatase inhibitors (Calbiochem). The protein samples were separated by SDS-PAGE, transferred to polyvinylidene difluoride (PVDF) membrane (Thermo Scientific), and detected with the indicated antibodies.

Chromatin immunoprecipitation (ChIP) and dot blot.

Cells were treated as indicated, crosslinked with 1% formaldehyde in culture media for 10 min, followed by quenching with 125 mM glycine. Cells were then permeabilized in swelling buffer (5 mM PIPES pH 8.0, 85 mM KCl, 0.5% nonidet P-40). Nuclei were resuspended in MNase digestion buffer (10 mM Tris pH 7.4, 15 mM NaCl, 60 mM KCl, 0.15 mM spermine, 0.5 mM spermidine) and 0.8 U/μl MNase (Thermo Scientific) was added for 30–45 min at 37 °C. The reaction was stopped by adding 50 mM EDTA, followed

by centrifugation. The nuclear pellets were resuspended in 10 mM Tris-HCl (pH8.0), 100 mM NaCl, 1mM EDTA, 0.5 mM EGTA, 0.1% Na-deoxycholate, 0.5% N-lauroylsarcosine. Lysates were sonicated briefly to disrupt nuclear membranes using an ultra sonicator with water bath (Bioruptor, Diagenode). Diluted lysates were incubated overnight at 4 °C with the indicated antibodies after addition of 1% Triton X-100. IPs were performed using Protein A/G magnetic beads (Pierce, 10 % v/v). Eluted DNA was purified with QIAquick PCR purification kit (Qiagen) according to the manufacturer instructions. Purified ChIP DNA was analyzed by qPCR using a LightCycler 480 II (Roche), see Table S2 for primer sequences. All ChIP samples were normalized to input. In ChIP-PCR quantification, the standard comparative cycle threshold method was used to measure the amount of DNA. Where indicated, input-corrected ChIP DNA content was further normalized to a control treatment. For dot blot analyses, ChIP DNA was denatured using 0.5 M NaOH and 1.5 M NaCl and equal sample volumes were loaded onto a Hybond N+ nitrocellulose membrane (GE Biosciences) using the Bio-Dot apparatus (BioRad). Unless noted otherwise, volumes loaded for IP samples were generally greater than volumes loaded for input samples to enhance signal to noise ratio. Enrichment was normalized to input and expressed as arbitrary units. Membranes were washed once with denaturing buffer and wash buffer (3x SSC), followed by UV-crosslinking (UV Stratalinker 1800, Stratagene) and blocking with 5x Denhardt's solution (Thermo Scientific) for 1 h at 37 °C. Hybridization with TelC-Biotin (Biotin-PEG2-CCCTAACCCTAALys-NH2, PNA Innovations Inc.) or Alu-Biotin (5' Biotin-GGCCGGGCGCGGTGGCTCACGCCTGTAATCCCAGCA) was performed at 37 °C overnight. Chemiluminescent Nucleic Acid Detection Module (Thermo Scientific Cat# 89880) was used for signal detection and images were acquired using ChemiDox XRS with Image Lab software (Bio-Rad). Signal intensities were quantified with ImageQuant TL software (GE Healthcare Life Sciences).

Telomere length measurement.

Q-FISH analysis was carried as described previously [39], metaphases were collected 72 h post siRNA transfection. In brief, cells were incubated with 0.1 μg/ml colcemid for 2 h at 37 °C, harvested and immediately incubated in 75 mM KCl for 15–20 min at 37 °C, fixed in ice-cold methanol and glacial acetic acid (3:1) and dropped onto glass slides. Metaphase spreads were hybridized with Cy3-labelled PNA $(CCCTAA)_3$ (0.5 μg/ml, Panagene), washed, and mounted with ProLong Gold anti-fade reagent (Invitrogen). Images were captured using Cytovision software (Applied Imaging) on a fluorescence microscope (Axio2; Carl Zeiss), followed by quantification of fluorescence signals of individual telomeres using ImageJ or the TFL-Telo software (gift from P. Lansdorp, Vancouver, BC). Representative data from at least 20 metaphases of each genotype were pooled and scored using Graphpad Prism (GraphPad). The frequencies of individual telomeres were plotted against the telomere signal intensity using arbitrary units.

T-SCE.

Chromosome-Orientation-FISH (CO-FISH) was used to measure T-SCE [24]. Briefly, cells were cultured in DMEM medium containing 3:1 ratio of BrdU:BrdC (Sigma) at a final concentration of 10 μM for approximately 20 h, and subsequently with 0.1 μg/ml colcemid for approximately 2 h before harvest. T-SCE frequencies were measured 64 h after

transfection with the indicated siRNAs. Metaphase spreads were prepared as described for Q-FISH, stained with Hoechst 33258, exposed to UV light, and digested with exonuclease III to remove newly synthesized DNA strands. Hybridization and wash conditions were identical to those described for telomere-FISH. Alexa Fluor 488-labelled $(TTAGGG)_3$ and Cy3-labelled PNA $(CCCTAA)_3$ probes (0.5 μg/ml, Panagene) were used for the detection of leading and lagging strands, respectively. Images were acquired on a Zeiss Axiovert 200M microscope. T-SCE was scored as a CO-FISH telomere signal split between the two chromatids of a metaphase chromosome.

C-circle analysis.

C-circle detection was performed as described previously [40]. In brief, 2.5×10^5 cells were collected and lysed using QCP buffer (50 mM KCl, 10 mM Tris-HCl pH 8.5, 2 mM $MgCl_2$, 0.5% v/v IGEPAL CA-630, 0.5% v/v Tween-20) with 0.2 mg/ml Proteinase K (Ambion) at 56 °C for 1 h, followed by incubation at 70 °C for 20 min. 30 ng of gDNA was used as template for rolling circle amplification by PCR (30 °C 4 h, 70 °C 20 min), using 7.5 U phi 29 polymerase with 1 mM dATG each (dATP, dTTP and dGTP) (New England Biolabs) in 20 μl volume. For dot blots, PCR products were loaded onto Hybond N+ nitrocellulose membrane (GE Biosciences) using the Bio-Dot apparatus (BioRad) and UV-crosslinked, followed by TelC-Biotin hybridization and signal detection as described above.

Histone dimer affinity assay.

Human H2A and macroH2A1$^{1-122}$ were cloned into a pET30-based vector harboring an N-terminal, TEV protease-cleavable histidine tag and a C-terminal Flag tag. Human histone H2B was cloned into a pET30-based vector harboring an N-terminal HRV 3C protease-cleavable histidine tag. The recombinant histones were separately expressed in BL21 (DE3) E. coli cells and purified under denaturing conditions as previously described [41]. During the purification and renaturation into histone dimers the N-terminal histidine tags are proteolytically cleaved (TEV obtained from Promega, cat. V610A and HRV 3CN obtained from Pierce, cat. 1896490) yielding histones with native, “scarless”, N-terminal tails [41]. Refolded H2A-H2B dimers or macroH2A1$^{1-122}$-H2B dimers (2.5 μg) were incubated with Anti-Flag M2 affinity gel (A2220, Sigma) equilibrated in binding buffer (20 mM Hepes (pH7.9), 300 mM NaCl, 0.1 mM EDTA, 10% glycerol, 0.1% Tween-20, 0.5 mM DTT, 0.1 mg/ml BSA) with agitation at 4°C. The histone-bound beads were then incubated with 250 μg of HeLa S3 nuclear extract (NE) for 2 hours in nuclear extract binding buffer (20 mM Hepes (pH 7.9), 450 mM NaCl, 2 mM EDTA, 10% glycerol, 0.1% Tween-20, 0.5 mM DTT) with agitation at 4°C. The beads were then washed three times in NE binding buffer before elution of the histone dimer-bound complexes with elution buffer (20 mM Hepes (pH 7.9), 50 mM NaCl, 0.1 mM EDTA, 10% glycerol, 0.1% Tween-20, 0.5 mM DTT, 200 μg/ml Flag peptide (F3290, Sigma)). The eluted material was separated by SDS-PAGE with an NE standard curve, transferred to nitrocellulose and immunoblotted.

Statistics and Reproducibility

Statistical comparisons between replicate experiments were performed based on Student’s two-tailed t-test, paired t-tests where used for paired data sets. The Mann-Whitney U test

was used for comparison of data sets that do not assume a normal distribution. One-way analysis of variance (ANOVA) was used for comparison of Q-FISH data sets. Relevant statistical tests are indicated in the Figure legends. Statistical significance was set to $p \leq 0.05$. The number of independent replicates is listed for each experiment, sample sizes are indicated where appropriate. For box plots, bottom and top hinges denote first and third quartile, respectively, whiskers extend to 1.5 x the interquartile range and lines represent the median.

Data Availability Statement

Raw data and image files are available upon request.

Supplementary Material

Refer to Web version on PubMed Central for supplementary material.

Acknowledgments

We thank Julie Cooper for critical reading of the manuscript, T. Karpova for imaging support and R. A. Greenberg for reagents. R. J. G. acknowledges support from the Medical Research Council, grant number MC_UU_12025/unit program MC_UU_12009/3. This work was supported by the National Institutes of Health (NIH) training grant T32 GM007491–38 (P. D. R.) and grant R01 CA155232 (M. J. G.), and the Intramural Research Programs of the NIH National Cancer Institute, Center for Cancer Research and the National Institute on Aging.

References, Methods-only References

1. O'Sullivan RJ & Almouzni G Assembly of telomeric chromatin to create ALTernative endings. Trends Cell Biol 24, 675–85 (2014). [PubMed: 25172551]
2. Pickett HA & Reddel RR Molecular mechanisms of activity and derepression of alternative lengthening of telomeres. Nat Struct Mol Biol 22, 875–80 (2015). [PubMed: 26581522]
3. Dilley RL & Greenberg RA ALTernative Telomere Maintenance and Cancer. Trends Cancer 1, 145–156 (2015). [PubMed: 26645051]
4. Heaphy CM et al. Altered telomeres in tumors with ATRX and DAXX mutations. Science 333, 425 (2011). [PubMed: 21719641]
5. Lovejoy CA et al. Loss of ATRX, genome instability, and an altered DNA damage response are hallmarks of the alternative lengthening of telomeres pathway. PLoS Genet 8, e1002772 (2012). [PubMed: 22829774]
6. Clynes D et al. Suppression of the alternative lengthening of telomere pathway by the chromatin remodelling factor ATRX. Nat Commun 6, 7538 (2015). [PubMed: 26143912]
7. Napier CE et al. ATRX represses alternative lengthening of telomeres. Oncotarget 6, 16543–58 (2015). [PubMed: 26001292]
8. Nguyen DT et al. The chromatin remodelling factor ATRX suppresses R-loops in transcribed telomeric repeats. EMBO Rep 18, 914–928 (2017). [PubMed: 28487353]
9. O'Sullivan RJ et al. Rapid induction of alternative lengthening of telomeres by depletion of the histone chaperone ASF1. Nat Struct Mol Biol 21, 167–74 (2014). [PubMed: 24413054]
10. Leung JW et al. Alpha thalassemia/mental retardation syndrome X-linked gene product ATRX is required for proper replication restart and cellular resistance to replication stress. J Biol Chem 288, 6342–50 (2013). [PubMed: 23329831]
11. Goldberg AD et al. Distinct factors control histone variant H3.3 localization at specific genomic regions. Cell 140, 678–91 (2010). [PubMed: 20211137]
12. Ratnakumar K et al. ATRX-mediated chromatin association of histone variant macroH2A1 regulates alpha-globin expression. Genes Dev 26, 433–8 (2012). [PubMed: 22391447]

13. Wong LH et al. ATRX interacts with H3.3 in maintaining telomere structural integrity in pluripotent embryonic stem cells. Genome Res 20, 351–60 (2010). [PubMed: 20110566]
14. Khurana S et al. A macrohistone variant links dynamic chromatin compaction to BRCA1-dependent genome maintenance. Cell Rep 8, 1049–62 (2014). [PubMed: 25131201]
15. Kustatscher G, Hothorn M, Pugieux C, Scheffzek K & Ladurner AG Splicing regulates NAD metabolite binding to histone macroH2A. Nat Struct Mol Biol 12, 624–5 (2005). [PubMed: 15965484]
16. Kim J et al. Replication Stress Shapes a Protective Chromatin Environment across Fragile Genomic Regions. Mol Cell 69, 36–47 e7 (2018). [PubMed: 29249653]
17. Bouwman P et al. 53BP1 loss rescues BRCA1 deficiency and is associated with triple-negative and BRCA-mutated breast cancers. Nat Struct Mol Biol 17, 688–95 (2010). [PubMed: 20453858]
18. Bunting SF et al. 53BP1 inhibits homologous recombination in Brca1-deficient cells by blocking resection of DNA breaks. Cell 141, 243–54 (2010). [PubMed: 20362325]
19. Xu Y et al. 53BP1 and BRCA1 control pathway choice for stalled replication restart. Elife 6(2017).
20. Dilley RL et al. Break-induced telomere synthesis underlies alternative telomere maintenance. Nature 539, 54–58 (2016). [PubMed: 27760120]
21. Porro A, Feuerhahn S, Reichenbach P & Lingner J Molecular dissection of telomeric repeat-containing RNA biogenesis unveils the presence of distinct and multiple regulatory pathways. Mol Cell Biol 30, 4808–17 (2010). [PubMed: 20713443]
22. Henson JD et al. DNA C-circles are specific and quantifiable markers of alternative-lengthening-of-telomeres activity. Nat Biotechnol 27, 1181–5 (2009). [PubMed: 19935656]
23. Poole LA et al. SMARCAL1 maintains telomere integrity during DNA replication. Proc Natl Acad Sci U S A 112, 14864–9 (2015). [PubMed: 26578802]
24. Bailey SM, Brenneman MA & Goodwin EH Frequent recombination in telomeric DNA may extend the proliferative life of telomerase-negative cells. Nucleic Acids Res 32, 3743–51 (2004). [PubMed: 15258249]
25. Nabetani A, Yokoyama O & Ishikawa F Localization of hRad9, hHus1, hRad1, and hRad17 and caffeine-sensitive DNA replication at the alternative lengthening of telomeres-associated promyelocytic leukemia body. J Biol Chem 279, 25849–57 (2004). [PubMed: 15075340]
26. Cho NW, Dilley RL, Lampson MA & Greenberg RA Interchromosomal homology searches drive directional ALT telomere movement and synapsis. Cell 159, 108–121 (2014). [PubMed: 25259924]
27. Pan X et al. FANCM, BRCA1, and BLM cooperatively resolve the replication stress at the ALT telomeres. Proc Natl Acad Sci U S A 114, E5940–E5949 (2017). [PubMed: 28673972]
28. Ramamoorthy M & Smith S Loss of ATRX Suppresses Resolution of Telomere Cohesion to Control Recombination in ALT Cancer Cells. Cancer Cell 28, 357–69 (2015). [PubMed: 26373281]
29. Conomos D, Reddel RR & Pickett HA NuRD-ZNF827 recruitment to telomeres creates a molecular scaffold for homologous recombination. Nat Struct Mol Biol 21, 760–70 (2014). [PubMed: 25150861]
30. Juhasz S, Elbakry A, Mathes A & Lobrich M ATRX Promotes DNA Repair Synthesis and Sister Chromatid Exchange during Homologous Recombination. Mol Cell 71, 11–24 e7 (2018). [PubMed: 29937341]
31. Clynes D et al. ATRX dysfunction induces replication defects in primary mouse cells. PLoS One 9, e92915 (2014). [PubMed: 24651726]
32. Huh MS et al. Compromised genomic integrity impedes muscle growth after Atrx inactivation. J Clin Invest 122, 4412–23 (2012). [PubMed: 23114596]
33. Watson LA et al. Atrx deficiency induces telomere dysfunction, endocrine defects, and reduced life span. J Clin Invest 123, 2049–63 (2013). [PubMed: 23563309]
34. Ishov AM, Vladimirova OV & Maul GG Heterochromatin and ND10 are cell-cycle regulated and phosphorylation-dependent alternate nuclear sites of the transcription repressor Daxx and SWI/SNF protein ATRX. J Cell Sci 117, 3807–20 (2004). [PubMed: 15252119]

35. Berube NG, Smeenk CA & Picketts DJ Cell cycle-dependent phosphorylation of the ATRX protein correlates with changes in nuclear matrix and chromatin association. Hum Mol Genet 9, 539–47 (2000). [PubMed: 10699177]

36. Minocherhomji S et al. Replication stress activates DNA repair synthesis in mitosis. Nature 528, 286–90 (2015). [PubMed: 26633632]

37. Buschbeck M & Hake SB Variants of core histones and their roles in cell fate decisions, development and cancer. Nat Rev Mol Cell Biol 18, 299–314 (2017). [PubMed: 28144029]

38. Kim JK, Oberdoerffer P & Khurana S The histone variant macroH2A1 is a splicing-modulated caretaker of genome integrity and tumor growth. Mol Cell Oncol 5(2018).

39. Wan B et al. SLX4 assembles a telomere maintenance toolkit by bridging multiple endonucleases with telomeres. Cell Rep 4, 861–9 (2013). [PubMed: 24012755]

40. Henson JD et al. The C-Circle Assay for alternative-lengthening-of-telomeres activity. Methods 114, 74–84 (2017). [PubMed: 27595911]

41. Ruthenburg AJ et al. Recognition of a mononucleosomal histone modification pattern by BPTF via multivalent interactions. Cell 145, 692–706 (2011). [PubMed: 21596426]

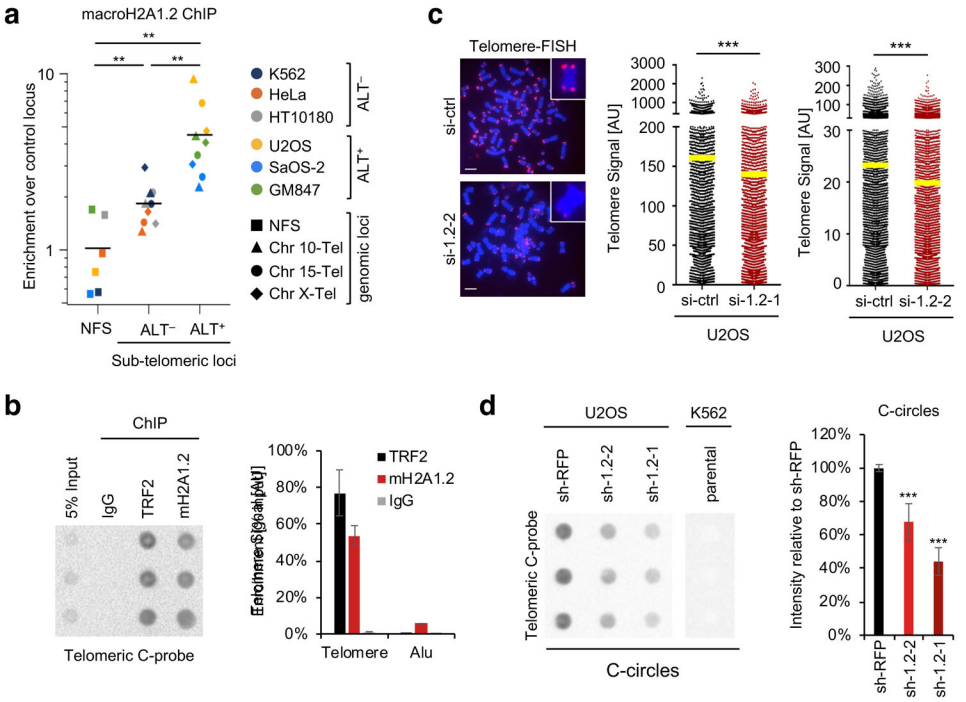

Figure 1. MacroH2A1.2 promotes telomere stability.

(A) MacroH2A1.2 ChIP in the indicated ALT$^+$ and ALT$^-$ tumor cell lines. Enrichment is shown for one non-fragile control site (NFS) and three sub-telomeric genomic regions, ChIP signal was normalized to a second, non-fragile control locus. Colors represent individual cell lines, shapes represent the indicated genomic loci, three samples were analyzed per cell line. * $p < 0.05$, ** $p < 0.01$, *** $p < 0.001$, based on Student's two-tailed t-test. (B) Dot blot for telomeric DNA content in indicated ChIP samples or input DNA from ALT$^+$ U2OS cells. Equal amounts of DNA were loaded for all samples. A quantification is shown for telomeric DNA and Alu repeat DNA probes (see Fig. S1). Values were normalized to input and represent mean and s.d. from 3 independent experiments. (C) Telomere Q-FISH in U2OS cells expressing control siRNA (si-ctrl) or one of two distinct siRNAs against macroH2A1.2 (si-1.2-1, si-1.2-2). Representative images show telomere signal (red) and metaphase chromosomes (blue), inlets depict individual chromosomes, scale bar: 5 μm. Telomere signal intensities were measured for at least 20 metaphases per genotype, each dot represents a single telomere, yellow lines indicate mean signal intensities, *** $p < 0.001$, based on one-way ANOVA. Graphs represent independent experiments. Similar results were obtained using a second ALT cell line (Fig. S1E, F). (D) C-circle analysis in U2OS cells expressing a control shRNA (sh-RFP), or two distinct shRNAs against macroH2A1.2 (sh-1.2-1, sh-1.2-2). K562 cells were included as a negative control. A quantification from three independent experiments is shown. Values are expressed as mean and s.e.m., *** $p < 0.001$, based on student's two-tailed t-test. Uncropped gel images are shown in Supplementary Data Set 1.

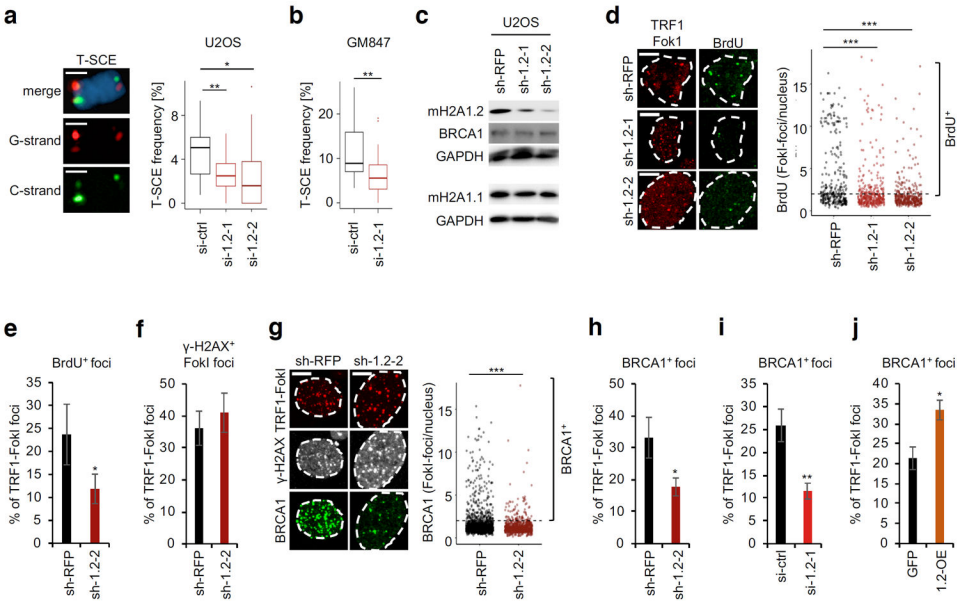

Figure 2. MacroH2A1.2 promotes homology-directed repair at telomeres.

(A) T-SCE as measured by CO-FISH in U2OS cells in the absence (si-ctrl) or presence of macroH2A1.2 knockdown using two distinct siRNAs, si-1.2-1 and si-1.2-2. Box plots depict % of T-SCE events per sister chromatid, * $p < 0.05$, ** $p < 0.001$, based on Student's two-tailed t-test. Representative CO-FISH images of a control metaphase chromosome are shown, scale bar: 2 μm. At least 20 metaphases were analyzed per sample. (B) T-SCE as in (A) in GM847 cells. (C) Western blot analyses in U2OS cells expressing shRFP, sh-1.2-1 or sh-1.2-2, see Supplementary Data Set 1 for uncropped blots. (D) Telomeric BrdU incorporation at TRF1-FokI-induced DSBs in U2OS cells expressing sh-RFP (n = 32 cells), sh-1.2-1 (n = 72 cells) or sh-1.2-2 (n = 70 cells). Representative IF images are shown, scale bar: 10 μm, *** $p < 0.001$ by Mann-Whitney U test. (E) Fraction of $BrdU^+$ TRF1-FokI foci from (D), values represent mean and s.e.m. from 5 independent experiments. (F) Fraction of γ-$H2AX^+$ TRF1-Fok1 foci in the presence of the indicated shRNA, values represent mean and s.e.m. from 6 independent experiments. (G) BRCA1 accumulation at TRF1-FokI-induced DSBs in U2OS cells expressing sh-RFP (n = 77 cells) or sh-1.2-2 (n = 60 cells). Representative IF images are shown, scale bar: 10 μm, *** $p < 0.001$ by Mann-Whitney U test. (H) Fraction of $BRCA1^+$ TRF1-FokI foci from (G), values represent mean and s.e.m. from 3 independent experiments. (I) Fraction of $BRCA1^+$ TRF1-FokI foci in U2OS cells expressing si-ctrl or si-1.2-1, values represent mean and s.e.m. (n = 6). (J) Fraction of $BRCA1^+$ TRF1-FokI foci in U2OS cells overexpressing macroH2A1.2 or eGFP. (E, H, I, J) * $p < 0.05$, ** $p < 0.01$, based on Student's paired, two-tailed t-test.

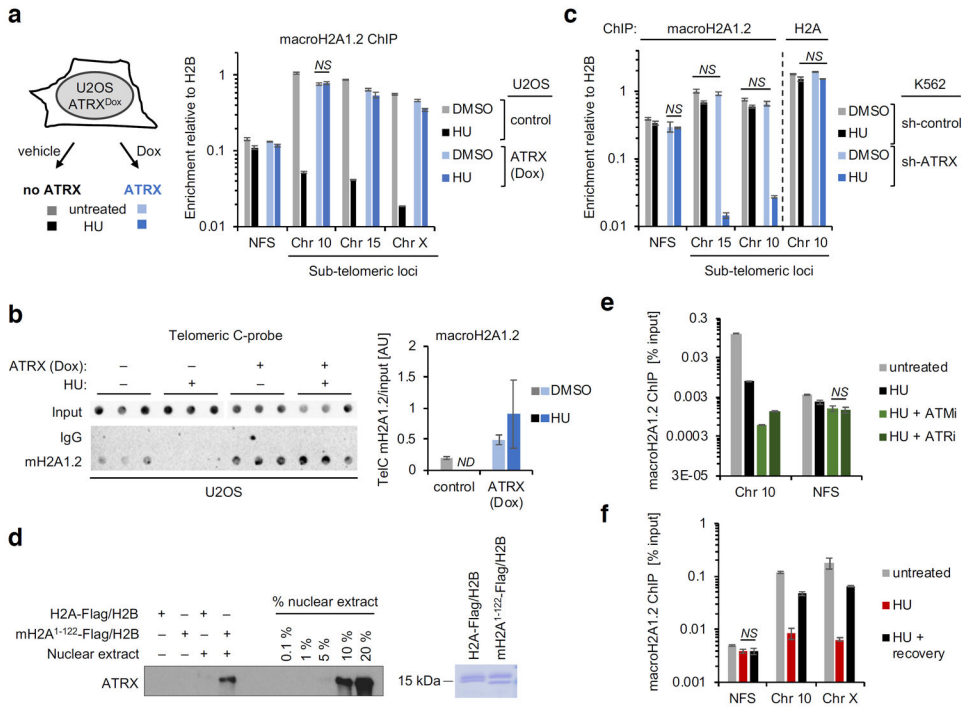

Figure 3. ATRX modulates macroH2A1.2 accumulation at telomeres during RS.

(A) MacroH2A1.2 ChIP at the indicated sub-telomeric loci in the presence or absence of RS in U2OS cells carrying a Dox-inducible ATRX transgene. Cells were either treated with vehicle (control) or Dox (ATRX) prior to HU treatment. Enrichment relative to histone H2B is shown for the indicated loci, see Fig. S3A for H2B ChIP. Values represent mean and s.d. from 3 independent experiments. (B) Dot blot for telomeric DNA content in the indicated ChIP or input samples from (A). Signal intensities for macroH2A1.2 ChIP were normalized against input, values represent mean and s.d. from 3 independent experiments. (C) ChIP for macroH2A1.2 or H2A in the presence or absence of HU in ALT-negative K562 cells expressing a control shRNA or sh-ATRX. Enrichment relative histone H2B is shown for the indicated loci. Values represent mean and s.d. from 3 independent experiments. See Fig. S3E for corresponding telomere dot blot. (D) Affinity purification of recombinant histone dimers containing H2B and either H2A or the histone-like region of macroH2A1 (mH2A1$^{1-122}$) using HeLaS3 nuclear extracts. Eluates and input samples were probed for ATRX. (E) MacroH2A1.2 ChIP at the indicated loci in the presence or absence of HU with or without ATM or ATR kinase inhibition (ATMi or ATRi). Values represent mean and s.d. from 3 independent experiments. See Fig. S3G for corresponding telomere dot blot. (F) MacroH2A1.2 ChIP at the indicated loci, before, during and 6 h after HU treatment. Values represent mean and s.d. from 3 independent experiments. For ChIP analyses, all pair-wise comparisons are significant based on Student's two-tailed t-test ($p < 0.05$), except when marked *NS* (not significant). Uncropped gel images are shown in Supplementary Data Set 1.

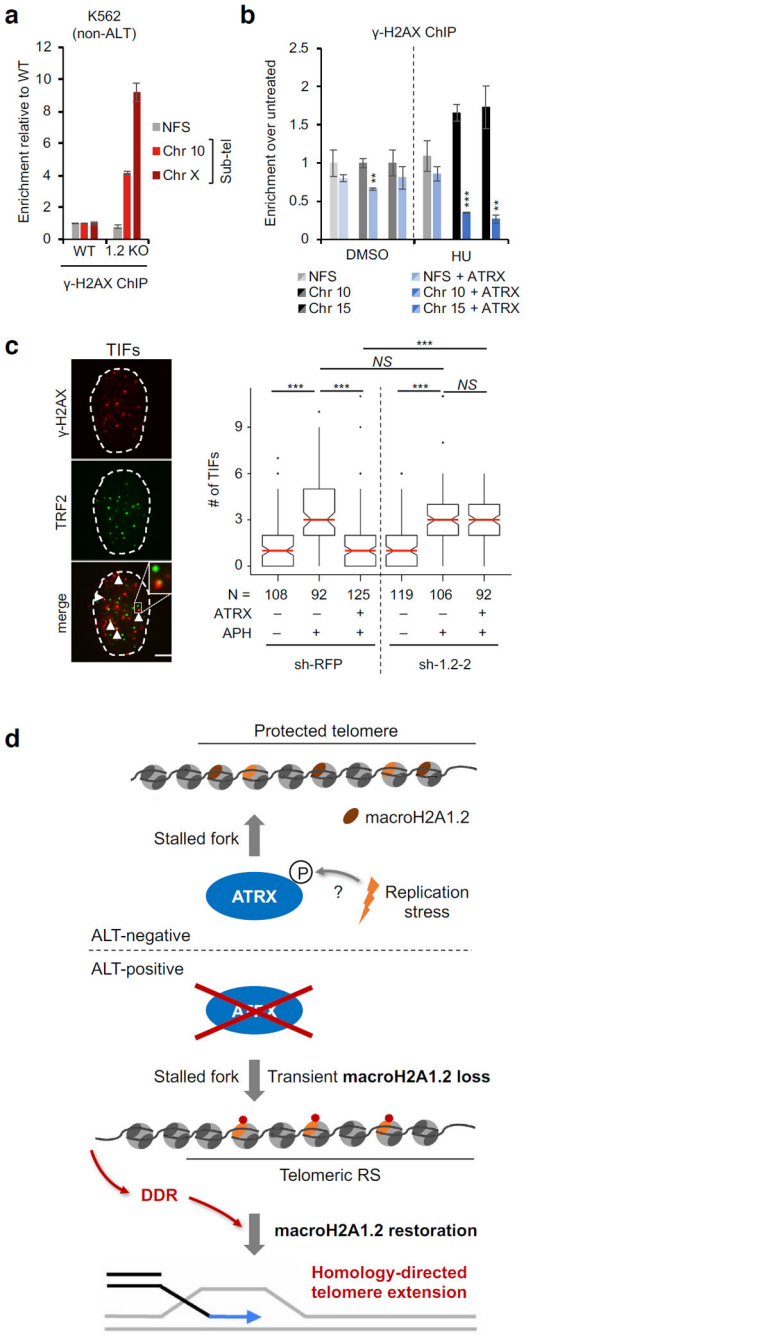

Figure 4. ATRX and macroH2A1.2 cooperate to protect from RS-induced telomere damage.

(A) ChIP for γ-H2AX at the indicated loci in K562 cells in the presence (WT) or absence of macroH2A1.2 (1.2 CRISPR-KO). Samples were normalized to untreated WT samples, values represent mean and s.d. from 3 independent experiments. See Fig. S4A for macroH2A1.2 ChIP. (B) γ-H2AX ChIP at the indicated loci in U2OS cells treated with vehicle (DMSO) or HU in the presence or absence of ATRX re-expression. Values represent mean and s.d. from 3 independent experiments. (C) Frequency of TIFs in U2OS cells with ATRX induction in the presence or absence of Aph, TIFs were defined based on co-

localization of γ-H2AX (red) and TRF2 (green), a representative image from Aph-treated, sh-RFP expressing U2OS cells is shown; scale bar = 5 μm. Box plots depict the number of TIFs per cell. N: number of cells. *** $p < 10^{-8}$ by Mann-Whitney U test, one of two independent experiments is shown. (D) Model linking ATRX and macroH2A1.2 to ALT telomere maintenance. ATRX-dependent macroH2A1.2 retention at stalled replication forks protects from excessive DNA damage in ALT-negative cells. In ALT-positive cells, ATRX deficiency leads to macroH2A1.2 loss and DSBs in response to RS, which triggers DDR-dependent macroH2A1.2 re-deposition to facilitate HR. In the absence of RS, lack of ATRX has little effect on telomeric macroH2A1.2 levels, pointing to DNA damage-induced modulation of ATRX function, which may involve ATRX phosphorylation in S phase (see discussion) [35].